Pattern Recognition 48 (2015) 3371–3384

Contents lists available at ScienceDirect

Pattern Recognition

journal homepage: www.elsevier.com/locate/pr

Face recognition under pose variation with local Gabor features enhanced by Active Shape and Statistical Models

Leonardo A. Cament [a,b], Francisco J. Galdames [a,b], Kevin W. Bowyer [c], Claudio A. Perez [a,b,*]

[a] Image Processing Laboratory, Department of Electrical Engineering, Universidad de Chile, Av. Tupper 2007, Santiago, Chile
[b] Advanced Mining Technology Center, Universidad de Chile, Av. Tupper 2007, Santiago, Chile
[c] Computer Vision Research Laboratory, Department of Computer Science and Engineering, University of Notre Dame, IN 46556, USA

ARTICLE INFO

Article history:
Received 30 November 2014
Received in revised form
25 April 2015
Accepted 19 May 2015
Available online 29 May 2015

Keywords:
Face recognition across pose
Statistical model for face recognition
Active shape model
Gabor features
Entropy weighting

ABSTRACT

Face recognition is one of the most active areas of research in computer vision. Gabor features have been used widely in face identification because of their good results and robustness. However, the results of face identification strongly depend on how different are the test and gallery images, as is the case in varying face pose. In this paper, a new Gabor-based method is proposed which modifies the grid from which the Gabor features are extracted using a mesh to model face deformations produced by varying pose. Also, a statistical model of the scores computed by using the Gabor features is used to improve recognition performance across pose. Our method incorporates blocks for illumination compensation by a Local Normalization method, and entropy weighted Gabor features to emphasize those features that improve proper identification. The method was tested on the FERET and CMU-PIE databases. Our literature review focused on articles with face identification with wide pose variation. Our results, compared to those of the literature review, achieved the highest classification accuracy on the FERET database with 2D face recognition methods. The performance obtained in the CMU-PIE database is among those obtained by the best methods published.

1. Introduction

Face recognition has a wide range of possible applications from person identification and surveillance to electronic marketing and advertising for selected customers. Face recognition in real time is a topic of active research, and several methods have been proposed to perform this task [1–4].

Most studies focus on frontal face recognition, reaching high accuracy on internationally available face databases. An important number of studies have focused directly on face recognition under the assumption that the face has already been localized [5,6].

Among the most widely cited methods for face recognition based on feature extraction are Eigenfaces [7], based on Principal Component Analysis (PCA), Fisherfaces [8], based on Linear Discriminant Analysis (LDA), and methods based on Independent Component Analysis (ICA) [9,10]. In [11], the Local Binary Pattern (LBP) method was proposed, in which the face image is divided into square windows where a binary code is generated whenever a pixel exceeds the value of the average within the window. Also some papers report addressing the problem of face recognition in low resolution images [12]. This method uses a multidimensional scaling approach where low resolution images are embedded in a Euclidean space which is used to perform the matching between gallery and test images. Gabor wavelets [13–16] have been used to extract local features achieving outstanding results in face recognition.

Among the methods based on Gabor Wavelets are the Elastic Bunch Graph Matching (EBGM) method [17], the Gabor Fisher Classifier (GFC) [18], the Local Gabor Binary Pattern Histogram Sequence (LGBPHS) [19], the Histogram of Gabor Phase Patterns (HGPP) [20], Local Gabor Textons (LGT) [21], Learned Local Gabor Pattern (LLGP) [22], Local Gabor Binary Pattern Whitening PCA (LGBPWP) [23], and the Local Matching Gabor method (LMG) [24–27]. In [28], the face was divided into patches without overlap, and then the best patches were selected and weighted with an LDA strategy in a greedy search. Finally, the local scores of the patches were combined with a global score obtained from the low frequency components of the FFT applied to the whole face, including its external boundary. Magnitude and phase Gabor features were combined in [29]. The LBP operator was used on the Gabor magnitude features and the LXP operator (Local Xor Pattern) on the Gabor phase features. Then, the face was divided into regions, and histograms of each region were computed on

* Corresponding author at: Department of Electrical Engineering, Advanced Mining Technology Center, Universidad de Chile, Av. Tupper 2007, Santiago, Chile. Tel.: +56 2 29784207, fax: +56 2 6720162.
E-mail addresses: lcament@ing.uchile.cl (L.A. Cament), fgaldame@ing.uchile.cl (F.J. Galdames), kwb@cse.nd.edu (K.W. Bowyer), clperez@ing.uchile.cl (C.A. Perez).

http://dx.doi.org/10.1016/j.patcog.2015.05.017
0031-3203/

LGBP and LGXP features. Every region dimensionality was reduced using LDA, and finally the regions were compared with cosine distance. In [30], Gabor features in face images at higher and lower resolutions were used.

Face recognition under varying pose continues to be an area of active research. There are various approaches to solving this problem using 2D as well as 3D methods. Some methods use a single face as input and build a 3D model called the 3D Morphable Model [31–33]. The 3D Morphable Model is based on a vector space representation of faces built using vectors of shape and texture. The parameters of the models are computed using a set of Eigen vectors obtained previously by training with images from 3D scans. A fully automatic face frontalization method using a 3D model was introduced in [34]. It works for poses varying up to $\pm 45^\circ$ on the yaw axis and $\pm 30^\circ$ on the tilt axis. In [35], an automatic method was developed to find correspondences between 2D facial feature points and a 3D face model. The 3D face model built was then rotated to generate the frontal view.

In our literature review, we focused on 2D methods because they are widely used and are applicable in real time. Nevertheless, the goal of this work is to develop a more accurate recognition method for rotated faces, not to create the fastest possible implementation. There are several methods that use 2D techniques to perform face recognition across pose. A method that performs frontalization by dividing the face into different components is presented in [36]. Several methods use Active Appearance Models (AAM) to frontalize the face [37–39] and perform the match with a frontal face from a gallery set. In [40] the image is divided into non-overlapping patches and then a statistically aligned model is built for each patch to perform a warping in the region. Using the same idea of patches, the image is divided into non-overlapping patches and a statistical model is constructed on each one at the score level [41]. This method models how the matching score varies when the input face pose is at a certain angle. A face recognition Gabor-based method using a regressor with a coupled bias-variance tradeoff is proposed in [42]. In this method, a statistical model is built at the score level, as in [41]. Some methods use face representations in a latent space to perform the recognition [43,44]. In [45] a dictionary learning method designed for face recognition is presented.

Several recent papers have shown that the Local Matching Gabor (LMG) method [24] and its variants [25,26] reach the best results for frontal face recognition. In the LMG method, a total of 4172 Gabor jets are employed to extract features at five different spatial resolutions and eight different orientations. A Borda count method is used to compare the inner products between the Gabor jets from the input face image and the Gabor jets from faces in the gallery [46]. In our previous work based on Gabor-feature face classification [26], faces are normalized using the eye position for coronal axis rotations (on the same face plane). Also, our previously proposed method included weights for the Gabor jets using an entropy measure and a preprocessing step with Local Normalization (LN) yielding results that are among the best face classification results reported on the FERET and AR databases [25,26,47]. Our method performed competitively with other published methods on face occlusions and in the presence of noise. Nevertheless, for face poses with increasing angles out of the face plane, the face normalization step loses the correction effect and, as in most 2D face recognition methods, performance declines significantly. For example, methods reaching near 100% for frontal face recognition may drop by up to 40% with pose variations $\pm 60^\circ$ [40].

In this paper, a new method for face recognition under pose variation is proposed. This method uses Active Shape Models (ASM) [48] to reposition Gabor jets on the face according to face pose. Because of local changes in the 2D face image with varying pose, we also use a local statistical model [41] to compensate for face pose. These new extensions to our previous LMGEW method that uses entropy-weighted features and fusion among LMG and LBP features [26] yield significant improvements in face recognition under varying pose. We tested our method and its variants using the FERET and CMU-PIE databases, which are among the most used databases to evaluate methods of face recognition across pose. The FERET database has pose variation between $\pm 60^\circ$, and has been used in many recent publications of face recognition across pose [33–35,41–43,49]. According to our literature review, our method reached the highest classification performance published in the FERET database with 2D face recognition methods. The CMU-PIE database has pose variations near $\pm 90^\circ$ and also has been used in most recent publications of face recognition across pose [33–35,42,43,49–51]. The performance of our method on the CMU-PIE database is among those that reached the highest classification performance.

2. Methodology

Our proposed model for face recognition based on local matching Gabor consists of three main modules [24]: image alignment using ASM, feature extraction through Gabor jets

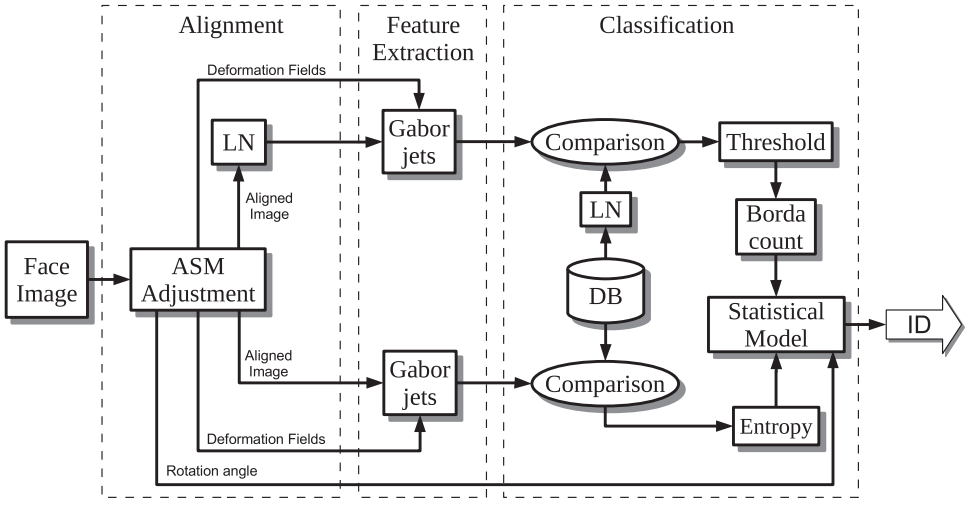

Fig. 1. The proposed method consists of three main modules: image alignment based on ASM, feature extraction through Gabor jets computation, and classification using entropy weights and statistical model matching.

computation, and classification using a statistical model, as shown in Fig. 1.

In the first module, an ASM is used to align the face and to determine its shape with the goal of extracting features from corresponding points relative to the gallery image. Also, an illumination compensation method called Local Normalization (LN) is used in the normalized image, as was shown to improve results in [47].

The second module performs the Gabor jet computation to extract face features. The spatial position for the computation of each Gabor jet is defined using the ASM adjusted to the face pose. A grid of Gabor jets is placed over the face using the eye positions as references as described in [24]. The grid is deformed using the ASM adjusted to the face. In this way, the position of the Gabor jets with respect to the face features (eyes, nose, mouth, etc.) is closer to the original position in the frontal face when the pose changes (see Fig. 4).

The third module carries out face classification. At this stage, entropy weights are introduced to weight each jet. A Borda count method is used [26] for classification and a local statistical model is employed to address pose change [41]. This local statistical model learns how the face texture varies as the face changes in pose. The model divides the face into several regions and the texture variation is computed for each region as the pose changes.

2.1. Pose detection and face alignment

2.1.1. Detection of face deformation by ASM

A deformable model is adjusted to the face in order to take pose changes into account. A linear statistical shape model called ASM is used [48]. This type of deformable model uses a linear transformation in a vector space, which takes the main configurations of the modeled shape in a set of examples taken into account. The model uses a Point Distribution Model (PDM), where the shape of the object is defined by a vector with the coordinates of a set of points:

$$S = \left[x_1, y_1, z_1, x_2, y_2, z_2 \ldots, x_l, y_l, z_l\right]^T \tag{1}$$

The shape S of a new object can be expressed as a mean shape S_0 deformed by the linear combination of basis vectors that represent the principal modes of variation of the object in a set of examples, and linearly deformed by an affine transformation. The shape S of a face in an image can be expressed as

$$S = \mathcal{T}(s, R, T; S_0 + \Psi_i p) \tag{2}$$

where p is a vector of parameters for the basis $\Psi = [S_1 | S_2 | \ldots | S_n]$ of n vectors, and $\mathcal{T}(s, R, T; \cdot)$ is a rigid transformation that performs a rotation by the rotation matrix $R(\alpha, \phi)$, scaling s, and translation by the vector $T = [t_x, t_y]^T$, i.e., if $\mathcal{T}(s, R, T; \cdot)$ is applied to a point $[x, y]^T$:

$$\mathcal{T}(s, R, T; [x, y]^T) = sR\begin{bmatrix} x \\ y \end{bmatrix} + T \tag{3}$$

The basis Ψ is built by a Principal Component Analysis (PCA) of a set of training shapes. Before performing the PCA, the training shapes are normalized by an iterative Procrustes analysis [52] to remove global variations, such as translation and rotation, and therefore taking into account only the non-rigid local variations in the PCA. The PCA provides a set of orthogonal modes of variation or eigenvectors, and its eigenvalues. The eigenvalues represent the importance of the corresponding eigenvector within the modes of variation across the training shapes. Among the eigenvectors, those with larger eigenvalues are selected to build the basis Ψ. Thus, a model that can generate large variations in shape using few parameters is obtained.

In order to fit the deformable model to the image, a particular type of ASM named Constrained Local Model (CLM) is used [53,54]. This CLM uses patches where local features are computed to search landmarks in the image. The position of each landmark is related to a point of the PDM. A set of training images is used to build a model that incorporates local features associated with each anatomical landmark. In order to fit the shape S to a test image by the CLM, the parameters of $\mathcal{T}(s, R, T; \cdot)$ and the vector of parameters, p, of the basis Ψ, are optimized (3). The optimization minimizes the difference between features computed in the patches at each point of S and the features of the model built using the training images. The image features are extracted from patches of the raw gray image, the image gradient, and local binary patterns (LBP).

The features computed in the test images are compared with the features of the training images by using the normalized correlation coefficient. Then, the method uses a non-parametric approach based on the mean-shift [55] mode seeking algorithm to

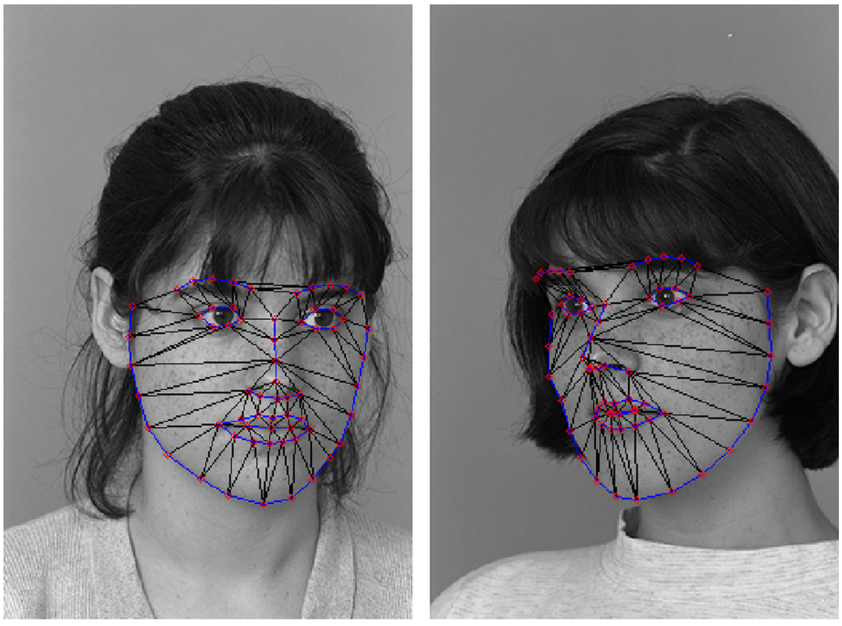

Fig. 2. Example of the mesh used to detect facial features by using the CLM method of Saragih et al. [54].

optimize the position of the points in the PDM by minimizing the difference between the training and test features. The result is a shape fitted to the facial features (Fig. 2). For a completely automatic face recognition system, pose and landmarks should be obtained automatically. However, for experimentation purposes, we assume them to be known beforehand, a common practice followed in several previous studies [24,31,37,40–43]. Therefore, the shapes adjusted by the ASM that did not fit correctly for large pose variations were adjusted manually to evaluate the expected performance of our proposed method.

2.1.2. Face alignment

Before computing the Gabor features, the images are normalized to a size of 300×400 pixels using the shapes adjusted to the face and a mean face shape. Fig. 3 shows the face mean shape (in blue lines) that is positioned on the face as follows: The vertex of the mean shape representing the position of the columella's base of the nose is positioned on the horizontal center of the image and at $1/3$ of the height of the image. The columella is the tissue that links the nasal tip to the nasal base, and separates the nares. It is the inferior margin of the nasal septum. The eyes are localized on the same horizontal line and their separation between centers is set to 68 pixels. The separation between the eyes controls the scale of the aligned mean shape and has the same scale used in [24]. In the alignment step, the images are rotated to set the eyes on the same horizontal line, scaled such that the width of the adjusted shapes is equal to the width of the aligned mean shape, and translated so that the center of the triangle formed by the center of each eye and the vertex at the columella of the nose coincide between the mean shape and the shapes adjusted to the faces. This alignment allows comparisons between gallery and test faces in similar positions, improving the performance of the method [26]. If the face pose has a large rotation (yaw rotation) and one side is occluded, the vertex at the upper part of the nose is used instead of the occluded eye. Fig. 3 shows a normalized image of the FERET database with the adjusted shape in green and the mean shape in blue.

2.2. Gabor features extraction with grid deformation

Gabor jets are computed on selected points, using five different grids with spatial scales defined by $0 \le \nu \le 4$. Our original method [26] used the grids defined in [24], where the images are normalized to 203×251 pixels with the eyes in fixed positions (67, 125) and (135, 125). Fig. 4(a) shows an image where the grid with spatial scale $\nu = 3$ is superimposed. Corresponding to the grid size, the Gabor filters have five spatial scales in the following equation:

$$\Psi_{\nu,\mu}(x,y) = \exp\left(-\frac{|\vec{k}|^2 |\vec{r}|^2}{2\sigma^2}\right)\exp\left(i\vec{k}\cdot\vec{r}\right) \tag{4}$$

where vectors $\vec{r} = \begin{bmatrix} x \\ y \end{bmatrix}$ and $\vec{k} = (\pi/2f^{\nu})\begin{bmatrix} \cos(\mu\pi/8) \\ \sin(\mu\pi/8) \end{bmatrix}$, and constants $f = \sqrt{2}$ and $\sigma = 2\pi$ [16]. The spatial scale is equivalent to $\lambda \in \left\{4, 4\sqrt{2}, 8, 8\sqrt{2}, 16\right\}$ in pixels [24].

At each point $p_{\nu}(i) = [x,y]$ on the grid corresponding to the scale ν, the Gabor wavelet has eight different orientations $0 \le \mu \le 7$ in (4). For the eight orientations, a set of Gabor features is extracted at each point on the grid and each set is called a jet:

$$G_{\mu}(p_{\nu}(i)) = [\Psi_{\nu,\mu} * I](p_{\nu}(i)), \tag{5}$$

where $*$ is the convolution operator and I is the image. These jets are normalized as

$$\overline{G}_{\mu}(p_{\nu}(i)) = \frac{|G_{\mu}(p_{\nu}(i))|}{\sqrt{\sum_{\mu=0}^{7} |G_{\mu}(p_{\nu}(i))|^2}}, \tag{6}$$

where $|\cdot|$ is the modulus of a complex number. Therefore, a jet can be represented by a vector of length 8 for each point $p_{\nu}(i)$.

The grids without deformation to locate Gabor jets as defined in [24] have very good performance in frontal faces [26]. Nevertheless, as in all 2D methods, the performance decreases significantly as the face varies in pose. A new method to correct the position of the Gabor jets for faces with varying pose is presented in this paper. First, the images are aligned as described in Section 2.1.2. Then, the positions of the Gabor jets are adjusted to compute them at the same relative position with respect to the facial features detected in each image by the adjusted shapes. The mean shape, S_0, is used to adjust the positions of the Gabor jets. The grids of Gabor jets are placed in the same position with respect to the mean shape for the aligned images of our original method [26]. In other words, the mean shape is a face normalized within a 203×251 pixel image, and the grids are positioned over it to be translated to the actual position of the mean shape in the alignment described in Section 2.1.2.

Fig. 4(a) shows an image of the FERET database with the mean face shape and the grid with $\nu = 3$ superimposed. Then, the grids are deformed by using the adjusted shape to change the positions at which the jets are computed in each image. A field of deformations $D(x,y) = [x', y']$ is computed using the Thin Plate Splines method [56] on the vertex of the model and adjusted shapes. This deformation field is the spatial transformation between the mean shape and the adjusted shapes, and it is used to deform the grid in such a way that the jets are computed at the same relative position with respect to the adjusted shapes of each image. Therefore, the positions of the points in the deformed grids are $p'_{\nu}(i) = D(p_{\nu}(i))$. Fig. 4(b) shows the grid with $\nu = 3$ deformed using this method. Fig. 4(c) and (d) shows deformed grids in a frontal and rotated face, respectively. As these figures show, the positions of the Gabor jets have the same relative position with respect to the face features in both images. If one side of the face is occluded because of the rotation, only the vertices and jets on the side of the face that is exposed are used to compute the deformation field and the Gabor features, respectively. The method assumes that a gallery is available with faces of the persons to be identified. For each face in the gallery, the Gabor jets are computed off-line and stored in a database for later on-line identification.

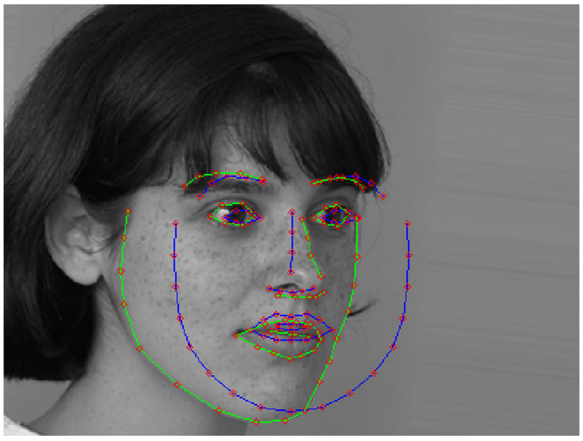

Fig. 3. Image from the FERET database normalized before using the face recognition method. The image is aligned using a mean face shape (blue/darker) and the shape adjusted to the face (green/lighter). The image is rotated to place the eyes on the same horizontal line, scaled such that the width of the adjusted shape is equal to the width of the mean shape, and translated so that the center of the triangle formed by the center of each eye and the vertex at the columella of the nose coincide. (For interpretation of the references to color in this figure caption, the reader is referred to the web version of this paper.)

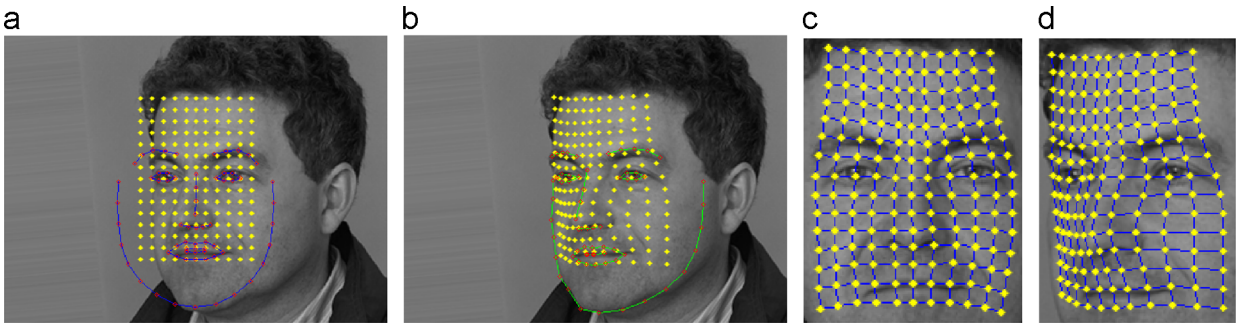

Fig. 4. Example of the deformation of the grids used to compute the Gabor jets. (a) Initial grid (yellow) and mean face shape (blue). The grid is set as if the mean face shape were a face normalized as described in [26]. (b) Deformed grid (yellow) and adjusted face shape (green). The original grid is deformed to have the same relative position with respect to the adjusted shape that the original grid has with respect to the mean shape. By using this deformation, the position of the Gabor jets has the same relative position with respect to the face features in different images. Figures (c) and (d) show the position of the Gabor jets in a frontal and rotated face, respectively. (For interpretation of the references to color in this figure caption, the reader is referred to the web version of this paper.)

2.3. Classification

2.3.1. Borda count

The third module, the Borda count matching, performs a comparison between the set of Gabor jets computed on the input face image and each set of Gabor jets stored in the gallery. The inner product between the input and gallery Gabor jets, which are vectors of length eight at each point of the five grids, is used in the comparison. The result of the inner products is a matrix of dimensions $N \times M$ called C, where N is the number of face images in the gallery and M is the number of jets. The final classification is performed using the Borda count method [46] which selects the identified face from the gallery according to a vote among all jets. Borda count is a voting method in which every voter ranks all the candidates in order of preference. Then, a sum of all voter ranks is performed to obtain the candidate scores. In our case, the voters are the Gabor jets, and the ranking is performed according to the inner products stored in C. Therefore, a ranking matrix, $O = \mathrm{BC}(C)$, is built using the values in each column of C. Finally, the identification score of the j-th gallery image with respect to the input image is

$$\mathcal{S}_j = \sum_{i=1}^{M} O_{ji} \tag{7}$$

The input image is classified using the highest classification score.

2.3.2. LN image computation

A preprocessing step is performed using our Local Normalization (LN) algorithm [47] on the images to obtain another set of Gabor features (Fig. 1). The LN algorithm is based on the work presented in [57], and the resulting normalized image is given by (8), where $I^{m\times m}_{mean}(x,y)$ denotes the mean of a neighborhood of $m \times m$ pixels around (x,y), and $I^{m\times m}_{std}(x,y)$ is the standard deviation in the neighborhood:

$$I_{ln}(x,y) = \frac{I(x,y) - I^{9\times 9}_{mean}(x,y)}{I^{9\times 9}_{std}(x,y) + 0.01} \tag{8}$$

The comparison matrix and ranking matrix for LN images are called C^{ln} and O^{ln}, respectively.

2.3.3. Borda Count Threshold

A Borda Count Threshold (BTH) is used to eliminate scores from Gabor jets with low values that act as noise in the identification procedure. A modified ranking matrix, $Q^{ln}_{j,i}$, is created by (9), where T_h is the threshold that eliminates noisy scores. This noisy score elimination has yielded significant improvements in classification results [25,26]:

$$Q^{ln}_{j,i} = \begin{cases} O^{ln}_{j,i} & \text{if } C^{ln}_{j,i} \geq T_h; \\ 0 & \text{if } C^{ln}_{j,i} < T_h. \end{cases} \tag{9}$$

Based on our previous work [25,26] the threshold was set to $T_h = 0.85$. The identification scores $\mathcal{S}_j$ are obtained using Q^{ln} instead of O (Eq. (7)), and the highest score denotes the person's identity.

2.3.4. Entropy weights

An entropy strategy [26,27] is used to emphasize the best performance features. An entropy vector E is computed using the comparison matrix C. The basic idea behind this computation is that, for a given jet, a probability, $P_{j,i}$, is defined in proportion to the comparison values with each enrolled person in the database as follows:

$$P_{j,i} = \frac{C_{j,i}}{\sum_{k=1}^{N} C_{k,i}}, \tag{10}$$

Shannon entropy of the i-th jet is computed using these probabilities as

$$E_i = -\sum_{j=1}^{N} P_{j,i} \log_2 P_{j,i} \tag{11}$$

The entropy is computed for each jet, creating the entropy vector, E. Because the values E_i are not uniformly distributed, the histogram of E is equalized. Then E is normalized to the range [0,1], and used to weight the ranking matrix in the computation of the identification score:

$$\mathcal{S}_j = \sum_{i=1}^{M} Q^{ln}_{ji}\, E_i, \tag{12}$$

2.3.5. Statistical model

Although the position where the jets are computed is corrected by deformation fields, the image is still 2D. Therefore, the Gabor features computed in images of the same person but with varying pose are different, mainly for large rotation angles. This variation of the Gabor features with respect to the angle can be modeled as follows: First, the probability distribution functions of the scores $\mathcal{S}_j$ with respect to the rotation angle are computed in different blocks defined in the grids. A training set of images is used to compute this probability. Then, the estimated probability is used to correct the scores $\mathcal{S}_j$ computed in an input image depending on its rotation angle.

The image is divided into $V \times H$ blocks as shown in Fig. 5, and a local probability model is built for each one. Instead of using all

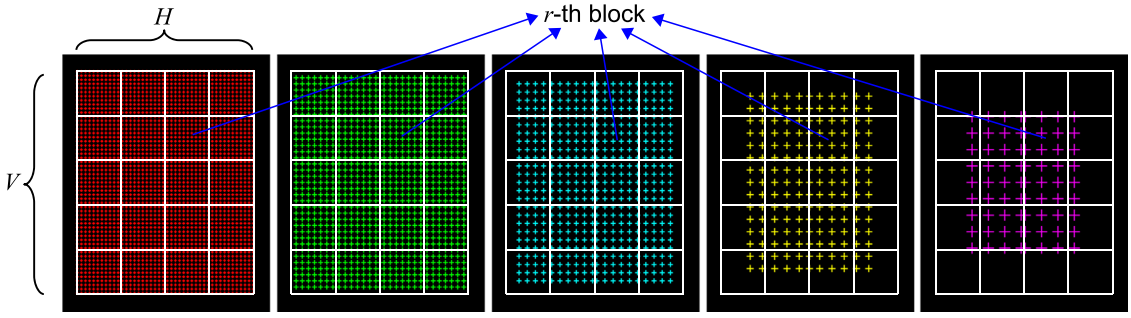

Fig. 5. Division in blocks for the statistical model. The five spatial scales used are shown. The white lines represent the different blocks and the + signs represent the spatial position where a Gabor jet is computed.

Fig. 6. Examples of face images taken from different view points for PIE (top) and FERET (bottom) databases. Images c25 and c09 taken with the camera located at an angle above the face. The other face images taken with a camera at the same height of the face. Face poses are shown only for left side rotation, right side rotation is analogous.

jets in the Borda count method, the Borda count is computed for each block individually in this approach. Thus, for the r-th block the comparison matrix C^r is extracted and the ranking matrix $O^r = \mathrm{BC}(C^r)$ is computed. The matrix C^r is a subset of the comparison matrix C that contains the inner product of the jets inside the r-th block. Note that if LN images are used, the matrices C and O are replaced by C^{ln} and O^{ln}, respectively. The identification score of the j-th gallery image in the r-th block $\mathcal{S}_j^r = \sum_{i=1}^{M_r} O_{ji}^r$, where M_r is the number of jets in the r-th block, is used as the input of the statistical model. The training and recognition are performed as follows:

Training: The prior distribution, $\mathcal{P}$, of the identification scores $\mathcal{S}^r$ with respect to a pose and matching label is computed for each block r. The pose label is the rotation angle ϕ_p, and the matching label w can take two values: *same* if the input and gallery images are of the same person, and *dif* if they are of different persons. Thus, the prior distribution is

$$\mathcal{P}\left(\mathcal{S}^r \mid w, \phi_p\right), w \in \{same, dif\} \tag{13}$$

The prior distribution is modeled by using a normal distribution as in [41]:

$$\mathcal{P}\left(\mathcal{S}^r \mid w, \phi_p\right) = \frac{1}{\sqrt{2\pi}\sigma_{w,p}^r} \exp\left[-\frac{1}{2}\left(\frac{\mathcal{S}^r - \mu_{w,p}^r}{\sigma_{w,p}^r}\right)^2\right] \tag{14}$$

where $\mu_{w,p}^r$, and $\sigma_{w,p}^r$ are, respectively, the mean and the standard deviation of the scores $\mathcal{S}^r$ for the r-th block, and across all the training images with rotation angle ϕ_p and matching label w. To obtain these values the training database must contain a gallery set and test sets labeled with angles ϕ_p. The Borda count scores $\mathcal{S}^r$ are computed for all test images, and the labels w and ϕ_p are assigned to compute $\mu_{w,p}^r$ and $\sigma_{w,p}^r$.

Recognition. To perform the recognition for the r-th block the Bayes rule is used:

$$\mathcal{P}\left(same \mid \mathcal{S}^r, \phi_p\right) = \frac{\mathcal{P}\left(\mathcal{S}^r \mid same, \phi_p\right)\mathcal{P}(same)}{\mathcal{P}\left(\mathcal{S}^r \mid same, \phi_p\right)\mathcal{P}(same) + \mathcal{P}\left(\mathcal{S}^r \mid dif, \phi_p\right)\mathcal{P}(dif)} \tag{15}$$

If the entropy is used in the classification, the weighting is not applied to each jet as in our LMGEW [26] method. In this case, an entropy is computed for each block. The entropy of the r-th block, E^r, is computed as the mean of the entropy of all jets inside the block. To use $\mathcal{P}$ in the computation of the identification score of the j-th gallery image with respect to the input image, the rotation angle, ϕ_p, of the input image is also needed. This angle can be considered as known for each input image, or computed by using the shape S adjusted to the face. Finally, the identification score of the j-th gallery image with respect to the input image is computed as

$$\mathcal{S}_j(\phi_p) = \frac{1}{VH}\sum_{r=1}^{VH} E^r \mathcal{P}\left(same \mid \mathcal{S}^r, \phi_p\right) \tag{16}$$

3. Database and experiments

The FERET and CMU-PIE databases were used to evaluate our method. Fig. 6 shows figures from PIE (top) and FERET (bottom) databases for negative angle poses. A brief description of the databases is given below.

3.1. The FERET database

The FERET database is the most widely used benchmark for face recognition methods [24]. It has a large number of images with different gesticulations, illumination, significant amount of time between pictures taken, and different face pose from -60° to $+60^\circ$. The FERET database is organized in 5 sets with frontal face images: the gallery is Fa, and the test sets are Fb, Fc, Dup1, Dup2. In the Fa set there are 1196 face images of different people. To test faces with varying pose, 8 sets from bb through bi were taken with the specific intention of investigating pose angle effects. Specifically, bf–bi are symmetric analogs of bb–be. The sets are bb, bc, bd, be, bf, bg, bh, and bi with pose angles 60°, 40°, 25°, 15°, -15°, -25° -40° and -60° respectively. The gallery set which has images in frontal pose was ba. Each of these sets has 200 images of 200 different people. Face images for FERET database, bb, bc, bd, be and ba sets, are shown in Fig. 6; Opposites sets, bf, bg, bh and bi, are analogs to those showed in Fig. 6.

3.2. The CMU-PIE database

The CMU-PIE database [58] is also one of the most commonly used databases for face recognition across pose variation. This database is composed of images of 68 different people. The images were acquired in 13 different poses, under 43 different illumination conditions, with 4 different expressions, and while the subjects were talking. To test our face recognition method, the 13 poses of each subject were used, corresponding to cameras 22, 02, 25, 37, 05, 09, 27, 07, 29, 11, 31, 14 and 34. Images with frontal illumination (flash 11) were used. Face images for PIE database, 22, 02, 25, 37, 05, 09 and 27 sets, are shown in Fig. 6; Opposites sets, 07, 29, 11, 31, 14 and 34, are analogs to those showed in Fig. 6.

3.3. Experiments

3.3.1. Grid deformation

The effectiveness of the ASM to deform the grid of Gabor filters to take into account pose variations was measured by the following experiments:

- Face identification performing only a face alignment, without using the grid deformation, as described in Section 2.1.2 and shown in Fig. 4(a).
- Face identification performing grid deformation, as described in Section 2.2 and shown in Fig. 4(b).

Both experiments were performed without any additional improvement of the LMG method so that only the improvement due to the grid deformation was measured. Then, the experiments were repeated using two different variants of our method to measure the improvement achieved by using each of them. These variants were introduced in our previous work [25–27,47], and the methods involved were presented in the previous section. The first variant includes a Borda count threshold (BTH) and an Entropy weighting (E), both presented in [25,26]. The BTH eliminates very small value scores that act as noise for the Borda count computation. The E weighting is used to emphasize the Gabor jets with the best performance. The second variant, in addition to BTH and E, includes the Local Normalization (LN) introduced in [47], which is used to compensate for illumination conditions.

3.3.2. Statistical model

The statistical model was trained for each block. Each of the FERET eight pose sets (bb, bc, bd, be, bf, bg, bh, bi) contains 200 images, including the gallery set. Each set was partitioned into two subsets, the first to train the model, and the second for testing. The training subsets were built by randomly choosing 100 images of the corresponding set, and the remaining 100 images were used to test the model. A cross-validation was performed exchanging the training and test sets, i.e., training with the second partition and testing with the first one. In the CMU-PIE database, an analogous procedure was carried out. Each of the 13 pose sets of the PIE database contains 68 images; therefore, 34 were randomly selected for the training set and 34 for the testing set to perform the cross-validation. The combinations of grid deformation, LN, BTH, and E with best performance in the previous experiments (Section 3.3.1), were used to evaluate the performance of the statistical model in each database. The method was tested using different numbers of blocks for the statistical model (see Fig. 5).

In order to measure the performance of the statistical model (P) in combination with the other methods used in our system, a set of experiments similar to those presented in Section 3.3.1 was performed. Face identification performing only a face alignment, or also using grid deformation, was carried out using P, and combinations of BTH, E, and LN.

3.3.3. Gallery sets with different pose angles

In order to measure the robustness of the method when images of rotated faces are used as gallery, different pose sets were enrolled. The sets bc, bd, be, bf, bg and bh of the FERET database were enrolled as gallery. The sets bb and bi were not used as gallery because one side of the face is usually not visible in these images due to the large rotation ($\pm 60^\circ$). In the CMU-PIE database, the sets of cameras 37, 05, 09, 27, 07, 29 and 11 were used as gallery, and the sets 22, 02, 25, 31, 14 and 34 were not used because of their large rotation. This experiment also allows comparison with other published methods in which the results are presented using rotated faces as galleries.

Table 1
Rank-1 results on the FERET database. The results of using only alignment (A), or grid deformation (GD) to compute the position of the Gabor jets were tested. These two methods were tested without including any other improvement, and using two variants of the LMG method. A first variant of our method includes Borda count with threshold (BTH) and Entropy weighting (E) of the Gabor jets. A second variant additionally includes a Local Normalization (LN) for illumination compensation.

Method	Set								
	bb (60°) (%)	bc (40°) (%)	bd (25°) (%)	be (15°) (%)	bf (-15°) (%)	bg (-25°) (%)	bh (-40°) (%)	bi (-60°) (%)	Mean (%)
A	34.5	84.0	96.5	99.5	100.0	98.5	74.0	36.5	77.9
GD	59.5	88.5	98.5	99.5	100.0	98.0	86.5	53.5	85.5
A+BTH+E	43.5	95.0	99.5	100.0	100.0	99.5	88.5	47.0	84.1
GD+BTH+E	71.0	94.5	99.0	99.5	100.0	99.5	94.5	67.5	90.7
A+LN+BTH+E	46.0	97.5	99.5	100.0	100.0	100.0	90.5	48.0	85.2
GD+LN+BTH+E	77.5	97.5	100.0	100.0	100.0	100.0	95.5	71.5	92.8

3.4. Results

3.4.1. Grid deformation results

Table 1 shows the Rank-1 results on the FERET database using only face alignment, or face alignment with grid deformation, and three different conditions. Both methods were tested without any other improvement of the LMG method, and then using the variants of the LMG which include BTH, E, and LN. As shown, the best results reach 100% for face pose near frontal, -25° to 25°. However, for larger pose changes, 40° or more, the identification results decrease significantly and differences among different variants of our method become evident. For example, when only alignment is used in images with pose variation of 60°, the correct identification rate is 34.5%. Using grid deformation, results improve to 59.5%. As shown in Table 1 the results obtained with grid deformation are significantly better than those obtained with only alignment. This improvement can be explained because with the grid deformation, the extracted features are closer to the features extracted in the frontal face enrolled in the gallery. This effect is especially noticeable in faces with large pose variation. If we combine BTH, LN, and E [26,47] with face alignment and grid deformation, the recognition rate improves significantly achieving the highest results. This improvement can be seen in Table 1, particularly for the $\pm 40^\circ$ and $\pm 60^\circ$ rotation angles. For example, the results using grid deformation (GD) increase 10% for the $\pm 40^\circ$ (GD+LN+BTH+E), and 32% for the $\pm 60^\circ$, if LN, BTH and E are used.

Table 2 shows the results of the same experiments described above but carried out using the PIE database. In same way as in the FERET database, the results are 100% for the near frontal poses (05, 09, 07, 29). However, for larger rotation angles the performance decreases. Results obtained using grid deformation are always better than those with alignment only. The best performance was obtained using grid deformation with BTH and E, in this database. The performance did not improve when LN was used. For example, the performance obtained using grid deformation increased approximately 43.5% for the largest rotation angles (sets 22 and 34) when BTH and E were used, but it increased only 28.2% if BTH, E and LN were used.

3.4.2. Statistical model results

Table 3 shows the results of the classification performance on the FERET database for different arrays of blocks used to test the statistical model. The best result was reached with an array size of 20×25, therefore this size was selected for further testing of the statistical model. Table 4 shows analogous results on the CMU-PIE database. The best result for the PIE database was achieved with an array size of 8×10, accordingly this size was selected for further testing on the PIE database.

Table 5 shows the results of face identification using only face alignment, or face alignment with grid deformation, with P and combinations of BTH, E, and LN in the FERET database. Results show that the use of the statistical model improves the recognition rate significantly, as can be seen by comparison with those in Table 1. The recognition rates reach 100% for near frontal images, and nearly 99% for $\pm 40^\circ$ pose angles. For $\pm 60^\circ$ pose angles the improvement is roughly 16% of the best result shown in Table 1.

Table 5 shows that the results using GD are always better than those using A. The best result was achieved by the combination DG+P+BTH+LN, with a mean performance of $96.4 \pm 0.2\%$. However, this performance was very close to that obtained by the combinations DG+P+BTH, DG+P+BTH+E and DG+P+BTH+LN+E. The results show that the improvement in the performance is similar using only BTH, or combinations of BTH, E and LN.

The performance obtained in the FERET database by our previous work [26] is shown in Table 5 with the options A+BTH+E. The mean performance increases from 84% to 96% using our new method. The improvement is greater if the extreme poses are considered. For example, taking into account the poses with $\pm 60^\circ$ the performance increases from 45.4% to 86.8%.

Table 6 shows the results of using P and combinations of BTH, E and LN on the CMU-PIE database. In the same way as on the FERET database, the results improved significantly by using the statistical model. Considering the experiments with better average results in Tables 2 and 6, the performance improvement in the largest rotation angles (sets 22 and 34) is 53% when the statistical model is used. Also the results using GD are always better than when using A.

The best performance was achieved using GD+P+BTH on the CMU-PIE database, with a mean performance of $87.1 \pm 1.5\%$ (Table 6). The performance of combination GD+P+BTH+E was close to this result, nevertheless, the combinations using LN did not improve the results.

Comparing our previous method (Table 6, options A+BTH+E) with the new one in the CMU-PIE database yields a mean performance improvement that goes from 73.4% to 87.4%. Comparing the extreme poses (sets 22 and 34), the performance increases from 28% to 54.5%.

3.4.3. Gallery sets with different pose angle results

Table 7 shows the results of enrolling sets of images with various pose angles, between -40° and 40°, as gallery in the FERET database. Results show that the highest recognition performance was reached consistently for faces with pose closest to the enrolled face angle. Even if faces with a small pose variation are used as gallery, the recognition rate of faces with large pose variation improves significantly. Using galleries with just $\pm 15^\circ$, the average result in the test sets with $\pm 60^\circ$ of rotation in the same direction is 94.6%.

Table 8 shows the results of using images with different pose angles as gallery in the CMU-PIE database. Also, the highest recognition rates were consistently reached for faces with pose angle closest to the enrolled faces. Using the sets of cameras 37

Table 2
Rank-1 results on the CMU-PIE database. The results of using only alignment (A), or grid deformation (GD) to compute the position of the Gabor jets were tested. These two methods were tested without including any other improvement and using two variants of the LMG method. A first variant of our method includes Borda count with threshold (BTH) and Entropy weighting (E) of the Gabor jets. A second variant additionally includes a Local Normalization (LN) for illumination compensation.

Method	Set												
	22 (%)	02 (%)	25 (%)	37 (%)	05 (%)	09 (%)	07 (%)	29 (%)	11 (%)	31 (%)	14 (%)	34 (%)	Mean (%)
A	25.0	54.4	51.5	95.6	100.0	100.0	100.0	100.0	69.1	55.9	38.2	22.1	67.6
GD	26.5	64.7	60.3	98.5	100.0	100.0	100.0	100.0	97.1	69.1	61.8	20.6	74.9
A+BTH+E	30.9	70.6	67.6	100.0	100.0	100.0	100.0	100.0	80.9	54.4	51.5	25.0	73.4
GD+BTH+E	42.6	79.4	76.5	98.5	100.0	100.0	100.0	100.0	98.5	72.1	57.4	25.0	79.2
A+LN+BTH+E	27.9	73.5	64.7	100.0	100.0	100.0	100.0	100.0	75.0	58.8	44.1	26.5	72.5
GD+LN+BTH+E	33.8	70.6	75.0	98.5	100.0	100.0	100.0	100.0	98.5	69.1	67.6	26.5	78.3

Table 3
Performance of the statistical model on the FERET database using different array sizes of $H \times V$ blocks. The grid deformation, LN, BTH, and E were used in the tests.

Arrays of block divisions	Set								
	bb (60°) (%)	bc (40°) (%)	bd (25°) (%)	be (15°) (%)	bf (−15°) (%)	bg (−25°) (%)	bh (−40°) (%)	bi (−60°) (%)	Mean (%)
4 × 5	87.0	99.2	100.0	99.5	100.0	100.0	97.8	81.9	95.7
8 × 10	87.4	99.5	100.0	99.9	100.0	100.0	97.9	83.0	95.9
12 × 15	87.5	99.5	100.0	99.8	100.0	100.0	97.7	84.3	96.1
16 × 20	88.6	99.5	100.0	99.7	100.0	100.0	97.9	82.0	96.0
20 × 25	89.3	99.3	100.0	100.0	100.0	100.0	97.9	84.2	96.3
24 × 30	88.5	99.5	100.0	100.0	100.0	100.0	97.9	81.5	95.9
28 × 35	87.9	99.5	100.0	100.0	100.0	100.0	98.5	82.4	96.0
32 × 40	88.0	99.5	100.0	100.0	100.0	100.0	98.1	82.3	96.0
36 × 45	87.4	99.4	100.0	100.0	100.0	100.0	98.2	81.0	95.8
40 × 50	87.2	99.5	100.0	100.0	100.0	100.0	98.3	81.5	95.8
44 × 55	86.6	99.4	100.0	100.0	100.0	100.0	97.8	81.6	95.7

Table 4
Performance of the statistical model on the CMU-PIE database using different array sizes of $H \times V$ blocks. The grid deformation, BTH and E were used in the tests.

Arrays of n° blocks	Set												
	22 (%)	02 (%)	25 (%)	37 (%)	05 (%)	09 (%)	07 (%)	29 (%)	11 (%)	31 (%)	14 (%)	34 (%)	Mean (%)
4 × 5	61.0	82.2	88.1	100.0	100.0	100.0	100.0	100.0	100.0	71.8	62.4	43.2	84.1
8 × 10	64.1	89.9	91.6	100.0	100.0	100.0	100.0	100.0	100.0	76.0	74.3	46.2	86.8
12 × 15	58.8	89.1	90.7	100.0	100.0	100.0	100.0	100.0	99.9	72.8	69.0	43.7	85.3
16 × 20	59.6	88.5	91.2	100.0	100.0	100.0	100.0	100.0	99.6	75.4	69.0	42.8	85.5
20 × 25	56.9	88.4	88.2	100.0	100.0	100.0	100.0	100.0	99.1	78.1	65.4	36.8	84.4
24 × 30	57.5	88.1	87.2	100.0	100.0	100.0	100.0	100.0	99.0	77.5	64.4	39.1	84.4
28 × 35	61.3	89.3	88.2	100.0	100.0	100.0	100.0	100.0	99.4	79.3	65.3	35.9	84.9
32 × 40	57.6	87.5	86.8	100.0	100.0	100.0	100.0	100.0	99.0	79.0	62.8	34.4	83.9
36 × 45	54.1	86.6	87.1	100.0	100.0	100.0	100.0	100.0	99.6	78.2	61.6	38.4	83.8
40 × 50	54.3	88.1	86.6	100.0	100.0	100.0	100.0	100.0	99.6	74.9	59.6	32.9	83.0
44 × 55	51.8	86.3	84.9	100.0	100.0	100.0	100.0	100.0	99.4	76.3	59.1	34.9	82.7

Table 5
Rank-1 results of the proposed methods in FERET database, using only alignment (A), or alignment with grid deformation (GD), with the statistical model (P) and combinations of a Borda count with threshold (BTH), Entropy weighting (E), and Local Normalization (LN).

Method	Set								
	bb (60°) (%)	bc (40°) (%)	bd (25°) (%)	be (15°) (%)	bf (−15°) (%)	bg (−25°) (%)	bh (−40°) (%)	bi (−60°) (%)	Mean (%)
A+P	56.2	96.2	100.0	100.0	100.0	100.0	95.0	56.9	88.0
GD+P	83.2	98.3	100.0	99.6	100.0	100.0	97.9	82.9	95.2
A+P+BTH	60.7	97.9	100.0	100.0	100.0	100.0	95.7	55.7	88.7
GD+P+BTH	87.4	98.9	100.0	99.7	100.0	100.0	99.0	83.4	96.0
A+P+BTH+E	58.8	97.7	100.0	100.0	100.0	100.0	96.1	55.3	88.5
GD+P+BTH+E	87.5	98.7	100.0	99.7	100.0	100.0	98.6	82.9	95.9
A+P+BTH+LN	58.8	98.7	100.0	100.0	100.0	100.0	95.7	59.9	89.1
GD+P+BTH+LN	89.0	99.5	100.0	100.0	100.0	100.0	98.1	84.6	96.4
A+P+BTH+LN+E	56.1	98.0	100.0	100.0	100.0	100.0	95.5	57.8	88.4
GD+P+BTH+LN+E	89.3	99.3	100.0	100.0	100.0	100.0	97.9	84.2	96.3

Table 6
Rank-1 results of the proposed methods in CMU-PIE database, using only alignment (A), or alignment with grid deformation (GD), with the statistical mode (P) and combinations of a Borda count with threshold (BTH), Entropy weighting (E), and Local Normalization (LN).

Method	Set												
	22 (%)	02 (%)	25 (%)	37 (%)	05 (%)	09 (%)	07 (%)	29 (%)	11 (%)	31 (%)	14 (%)	34 (%)	Mean (%)
A+P	38.4	79.7	74.6	100.0	100.0	100.0	100.0	100.0	91.9	62.5	51.6	31.8	77.5
GD+P	56.6	86.9	85.6	100.0	100.0	100.0	100.0	100.0	100.0	80.7	76.3	46.8	86.1
A+P+BTH	40.4	82.1	76.0	100.0	100.0	100.0	100.0	100.0	87.8	67.4	58.1	34.6	78.9
GD+P+BTH	61.2	90.9	92.2	100.0	100.0	100.0	100.0	100.0	100.0	79.0	74.3	47.5	87.1
A+P+BTH+E	37.6	80.0	75.4	100.0	100.0	100.0	100.0	100.0	87.6	65.3	52.9	34.6	77.8
GD+P+BTH+E	64.1	89.9	91.6	100.0	100.0	100.0	100.0	100.0	100.0	76.0	74.3	46.2	86.8
A+P+BTH+LN	40.9	81.3	74.4	100.0	100.0	100.0	100.0	100.0	90.0	66.3	54.0	35.1	78.5
GD+P+BTH+LN	55.3	87.4	89.0	100.0	100.0	100.0	100.0	100.0	100.0	80.1	77.6	45.1	86.2
A+P+BTH+LN+E	37.8	80.1	74.0	100.0	100.0	100.0	100.0	100.0	87.4	63.1	53.8	33.4	77.5
GD+P+BTH+LN+E	53.7	86.3	87.9	100.0	100.0	100.0	100.0	100.0	100.0	80.4	74.9	47.9	85.9

Table 7
Rank-1 performance for the method using galleries with different pose angles in FERET database. The GD, P, BTH and LN were used in the tests.

Yaw rotation of the gallery (deg)	Set									
	bb (60°) (%)	bc (40°) (%)	bd (25°) (%)	be (15°) (%)	ba (0°) (%)	bf (−15°) (%)	bg (−25°) (%)	bh (−40°) (%)	bi (−60°) (%)	Mean (%)
40	98.5	Gallery	99.5	99.5	99.2	99.0	92.8	77.0	34.4	87.5
25	99.3	99.5	Gallery	100.0	100.0	100.0	99.3	93.5	50.3	92.7
15	96.8	99.5	100.0	Gallery	100.0	100.0	99.1	96.5	66.2	94.8
0	89.0	99.5	100.0	100.0	Gallery	100.0	100.0	98.1	84.6	96.4
−15	69.2	99.3	100.0	100.0	100.0	Gallery	100.0	99.8	93.5	95.2
−25	49.0	93.5	98.8	99.3	100.0	100.0	Gallery	99.8	98.0	92.3
−40	25.5	76.8	89.0	96.3	96.4	99.0	99.5	Gallery	99.5	85.2

Table 8
Rank-1 performance for the method using galleries with different pose angles in the CMU-PIE database. The GD, P and BTH were used in the tests.

Gallery set	Set												
	22 (%)	02 (%)	25 (%)	37 (%)	05 (%)	09 (%)	27 (%)	07 (%)	29 (%)	11 (%)	31 (%)	14 (%)	34 (%)	Mean (%)
37	97.5	99.7	99.9	gallery	100.0	100.0	100.0	100.0	98.2	77.8	18.4	19.4	12.2	76.9
05	88.1	99.4	99.1	100.0	gallery	100.0	100.0	100.0	100.0	97.8	41.0	39.9	24.3	82.5
09	58.5	94.6	94.6	100.0	100.0	gallery	100.0	100.0	100.0	100.0	80.6	72.1	43.7	87.0
27	61.2	90.9	92.2	100.0	100.0	100.0	gallery	100.0	100.0	100.0	79.0	74.3	47.5	87.1
07	30.7	63.1	61.2	100.0	100.0	100.0	100.0	gallery	100.0	96.6	39.1	43.4	14.7	70.7
29	27.4	55.6	60.4	96.9	100.0	100.0	100.0	100.0	gallery	100.0	92.2	85.7	60.6	81.6
11	16.3	30.7	30.0	74.9	92.1	95.0	98.7	95.3	100.0	gallery	87.2	83.1	72.4	73.0

Table 9
Comparison of results with other 2D methods with face pose variations using the FERET database.

Method	Set									
	bb (60°) (%)	bc (40°) (%)	bd (25°) (%)	be (15°) (%)	ba (0°) (%)	bf (−15°) (%)	bg (−25°) (%)	bh (−40°) (%)	bi (−60°) (%)	Mean (%)
Ashraf et al. [40][a]	37.0	61.5	85.5	94.0	Gallery	97.0	88.5	67.0	40.0	71.3
Gao et al. [39]	44.0	81.5	93.0	97.0	Gallery	98.5	91.5	78.5	52.5	79.6
Gross et al. [59][a]	20	38	46	–	Gallery	–	44	45	8	33.5
Li et al. [42][a]	86.9	95.7	99	97.9	Gallery	95.9	96	90.9	78.1	92.5
Sarfraz and Hellwich [49][a]	78	90	95	–	Gallery	–	87	84	80	85.7
Sharma et al. [43]	70.0	82.0	94.0	95.0	Gallery	96.0	94.0	85.0	79.0	86.8
Vu and Caplier [41][a]	76.5	90.0	99.5	100.0	Gallery	100.0	99.0	95.5	87.0	93.4
Ours	89.0	99.5	100.0	100.0	Gallery	100.0	100.0	98.1	84.6	96.4

[a] Approximated values extracted from a graph.

and 11 as gallery, the average result in the sets with largest rotations is 86.1%.

3.5. Comparison with other methods

Our literature review focused on articles on face recognition with pose variation in the FERET and/or CMU-PIE databases. We extracted the results from those articles tables or figures. The best results obtained by those other methods are shown in Tables 9–12.

Table 9 shows the performance of 7 different 2D methods and our proposed method on the FERET database. Comparing the results, it can be concluded that our method reaches the highest overall classification performance.

Table 10 shows the performance of 5 different 3D methods and our proposed method on the FERET database. Some methods consider the set with 15° of rotation as the gallery. To perform an equivalent comparison with these methods, the sets with 15° and −15° of pose were used both individually and together as gallery. Our method outperformed all the methods that use the set with 0° of pose as gallery. Only one of the methods that uses the set with 15° of pose as gallery had a performance that exceeded that of our method, when we used the sets with 15° or −15° of pose as gallery individually [33]. Nevertheless, the sets in which our method is surpassed are only those with ±60° of face rotation. If we use both sets together (15° and −15°) as gallery, our method achieves the best performance. To use two sets as gallery, the rotation angle of the test face is computed by using the shape adjusted to the face, and then the comparison is carried out using the gallery set with the closest rotation angle.

Tables 11 and 12 show the results of our proposed method on the CMU-PIE database compared with other 2D and 3D methods, respectively. Since most publications show results in just some sets of the CMU-PIE database, the mean performance of our method is also shown considering only the sets used by each method. Accordingly, the last three columns of Tables 11 and 12 show different mean results: The first mean column "Mean[a]" shows the published performance of each method, the second mean column "Our mean[b]" shows the performance of our method considering only the sets used in the indicated paper, and the third column "Our mean[c]" shows the performance of our method when the sets c11 and c37 are used as gallery and only the sets used in the indicated paper are considered.

Table 11 shows the results of 10 different 2D methods and our proposed method on the CMU-PIE database. Our method is

Table 10
Comparison of results with 3D methods with face pose variations using the FERET database.

Method	Set									
	bb (60°) (%)	bc (40°) (%)	bd (25°) (%)	be (15°) (%)	ba (0°) (%)	bf (−15°) (%)	bg (−25°) (%)	bh (−40°) (%)	bi (−60°) (%)	Mean (%)
Asthana et al. [34]	–	90.5	98.0	98.5	Gallery	97.5	97.0	91.9	–	95.6
Blanz and Vetter [31]	94.8	95.4	96.9	99.5	Gallery	97.4	96.4	95.4	90.7	95.8
Ding et al. [35]	89.5	97.0	98.5	99.0	Gallery	98.5	98.0	94.5	78.0	94.1
Ours	89.0	99.5	100.0	100.0	Gallery	100.0	100.0	98.1	84.6	96.4
Paysan et al. [33]	97.4	99.5	100.0	Gallery	99.0	99.5	97.9	94.8	83.0	96.4
Romdhani [32]	92.7	99.5	99.5	Gallery	96.9	99.5	95.8	89.6	77.1	93.8
Ours (15°)	96.8	99.5	100.0	Gallery	100.0	100.0	99.1	96.5	66.2	94.8
Ours (−15°)	69.2	99.3	100.0	100.0	100.0	Gallery	100.0	99.8	93.5	95.2
Ours (15° and −15°)	96.8	99.5	100.0	Gallery	100.0	Gallery	100.0	99.8	93.5	98.5

Table 11
Comparison of results with other 2D Methods with face pose variations using the CMU-PIE database.

Method	Set															
	22 (%)	02 (%)	25 (%)	37 (%)	05 (%)	09 (%)	27 (%)	07 (%)	29 (%)	11 (%)	31 (%)	4 (%)	34 (%)	Mean[a] (%)	Our mean[b] (%)	Our mean[c] (%)
Asthana et al. [50]	–	–	–	89.4	95.5	98.5	Gallery	98.5	100.0	88.1	–	–	–	95.0	100.0	98.8
Castillo and Jacobs [51]	62	98	88	99	97	100	Gallery	99	99	97	91	93	60	90.2	87.1	94.1
Chai et al. [60]	–	–	–	82.4	98.5	98.5	Gallery	98.5	100.0	89.7	–	–	–	94.6	100.0	98.8
González-Jiménez et al. [37]	–	–	–	62	93	–	Gallery	–	93	75	–	–	–	80.8	100.0	100.0
Gross et al. [59][d]	39	59	57	89	94	95	Gallery	88	56	89	56	70	48	70.0	87.1	94.1
Kanade and Yamada [61]	50	100	85	100	100	100	Gallery	100	100	100	81	81	25	85.2	87.1	94.1
Li et al. [42][d]	73.5	100	88.3	100	100	100	Gallery	100	100	100	70.6	85.4	73.5	90.9	87.1	94.1
Prince et al. [62]	91	–	–	–	100	–	Gallery	–	–	–	–	–	–	95.5	80.6	98.8
Sarfraz and Hellwich [49][d]	36	78	80	86	88	92	Gallery	100	91	86	81	85	45	79.0	87.1	94.1
Sharma et al. [43]	79	88	85	100	100	100	Gallery	100	100	100	91	97	85	93.8	87.1	94.1
Ours	61.2	90.9	92.2	100.0	100.0	100.0	Gallery	100.0	100.0	100.0	79.0	74.3	47.5	87.1	–	–
Ours (c37 and c11)	97.5	99.7	99.9	gallery	100.0	100.0	100.0	95.3	100.0	Gallery	87.2	83.1	72.4	94.1	–	–

[a] Published mean performance of each method.
[b] Mean performance of our method considering the same sets as the comparison method.
[c] Mean performance of our method using the sets c37 and c11 as gallery and considering the same sets as the comparison method.
[d] Approximated values extracted from a graph.

Table 12
Comparison of results with 3D methods with face pose variations using the CMU-PIE database.

Method	Set															
	22 (%)	02 (%)	25 (%)	37 (%)	05 (%)	09 (%)	27 (%)	07 (%)	29 (%)	11 (%)	31 (%)	14 (%)	34 (%)	Mean[a] (%)	Our mean[b] (%)	Our mean[c] (%)
Asthana et al. [34]	–	–	–	97	100	100	Gallery	98.5	100	98.5	–	–	–	99.0	100.0	98.8
Blaz and Vetter [31][d]	79.5	–	–	–	97.5	–	Gallery	–	–	–	–	–	–	88.5	80.6	98.8
Ding et al. [35]	–	85.5	–	100	100	100	Gallery	100	100	100	–	77.6	–	95.4	95.7	96.4
Paysan et al. [33][d]	75.7	–	–	–	96.1	–	98.9 (Gallery)	–	–	–	–	–	–	90.2	80.6	99.2
Romdhani [32][d]	76	–	–	–	98	–	100 (Gallery)	–	–	–	–	–	–	91.3	80.6	99.2
Ours	61.2	90.9	92.2	100.0	100.0	100.0	Gallery	100.0	100.0	100.0	79.0	74.3	47.5	87.1	–	–
Ours (c37 and c11)	97.5	99.7	99.9	Gallery	100.0	100.0	100.0	95.3	100.0	Gallery	87.2	83.1	72.4	94.1	–	–

[a] Published mean performance of each method.
[b] Mean performance of our method considering the same sets as the comparison method.
[c] Mean performance of our method using the sets c37 and c11 as gallery and considering the same sets as the comparison method.
[d] Values computed with ambient light (set "light").

compared using the set with frontal faces (27) and also two sets with rotated faces (37 and 11) as gallery. By using the frontal faces as gallery, our method outperforms 6 of the 10 methods. This overall performance is caused by poor recognition in the sets with large rotation angles, although the performance in near frontal faces is 100%. If two sets of rotated faces are used as gallery, the performance of our method is increased, surpassing that of all the comparison methods.

Table 12 shows the performance of 5 different 3D methods and our method on the CMU-PIE database. The performance of our proposed method is shown using one and two sets as gallery. If only frontal faces are used in the gallery, our method outperforms

Table 13
Computational times of the method. FERET images and an ASM with 66 points were considered. The testing time of one image was computed using a gallery of 100 images.

Method	Testing time (seg.)
GD+P+BTH+LN+E	4.22
GD+P+BTH+LN	3.60
GD+P+BTH	3.42
GD+BTH	0.75

only 2 of the comparison methods. Nevertheless, when two sets are used in the gallery, our method outperforms 4 of the comparison methods.

Our method was tested on a standard PC with Intel Core i7-3770 CPU, 3.40 GHz × 8, and 16 Gb of RAM. The ASM and Thin Plate Splines methods are implemented in C++, and the other parts of our method are implemented in Matlab. Table 13 shows the computational time of our method with different configurations for the recognition of one face in the FERET database images. The statistical model uses the largest amount of time, followed by the Entropy weighting. This computational time can be significantly reduced by implementing the method in C++ instead of Matlab. Moreover, parallel processing can be implemented using GPU to reduce the computational time.

4. Conclusions

The LMG is a well-established method for frontal face identification with excellent performance. Nevertheless, as with most face identification methods, LMG performance declines significantly for large geometric deformations such as those produced by varying pose. In this study, a new method based on LMG is proposed using ASM to correct the position where Gabor jets are computed with pose changes. Also, the method incorporates a statistical model of the Borda count scores computed by using the Gabor jets. The method includes illumination compensation by Local Normalization, and an entropy weighting of the Gabor jets to emphasize those features most relevant for identification.

Our method was tested using the FERET and CMU-PIE databases, which are the most widely used international databases for face identification across pose. The FERET database has a subset with pose variations ($+60^\circ$, $+40^\circ$, $+25^\circ$, $+15^\circ$, $+0^\circ$, -15°, -25°, -40°, -60°) with 200 faces for each pose angle. Our method was tested enrolling each pose angle as the gallery set. Consistently the highest recognition performance was reached for faces with pose closest to the enrolled face angle. Also, even if a gallery with a small pose angle was used, the recognition rates of faces with high rotation improved significantly. The mean recognition rate of faces with $\pm 60^\circ$ of rotation increased from 86.8% to 95.2% if a gallery set with only 15° of rotation in the same direction was used. The mean improvement in the recognition rate of our method compared to the classical LMG on the FERET database for pose variation went from 77.9% to 96.4%.

As expected, the improvement was larger for significant face pose variation. For example, the mean performance of the classical LMG in faces with $\pm 60^\circ$ pose variation improved from 35.5% to 86.8% (144.5% improvement). The CMU-PIE database has 13 subsets with different pose variations, each with 68 faces. The recognition rate of faces with large rotation angles also improved significantly if a gallery with pose angle was used in this database. The recognition rate in the set with the largest rotation (set 22), increased from 61.2% to 97.5% when set 37 is used as gallery. Compared to the classical LMG, the mean performance in the recognition rate of our method on the CMU-PIE database increased from 67.6% to 87.1% when a gallery of frontal faces was used. The recognition rate improvement for the sets with largest rotation angles (22 and 34) was 130.8%.

Our results on the FERET database were compared to those of 12 different 2D and 3D state-of-the-art methods published previously. Our results were significantly better than all previous 2D methods which used the set with 0° of pose as gallery. The best 2D method [41] achieved a mean performance of 93.4%, while our method reached 96.4%. This difference was greater in faces with large pose variation angles. For example, the mean performance obtained in [41] for faces with $\pm 60^\circ$ of pose was 81.8% while our method results reached 86.8%. Only one of the 3D methods obtained a better mean result than our method on the FERET database [33]. This method uses the set with 15° of pose as gallery, and our method yields better results if we use the sets with $\pm 15^\circ$ of pose together as gallery. The 3D methods require a greater number of computations which can be interpreted as a disadvantage compared to our method.

In the CMU-PIE database, our method was compared with 10 different 2D and 5 different 3D previously published methods. Using the set with frontal faces as gallery the performance of our method outperforms 6 of the 2D methods. Nonetheless, if two sets with rotated faces (37 and 11) are used as galleries, the mean result of our method surpasses the performance of all previously published methods. If frontal faces are used in the gallery, the mean performance of our method is better than the performance of 2 of the 3D methods on the CMU-PIE database. Using the two sets with rotated faces as galleries, the mean performance of our method surpasses the results of 4 of the 5 methods.

Our proposed method has more consistent performance for the same rotation on the two tested databases (FERET and CMU-PIE) than the other comparison methods because methods that show highest performance on CMU-PIE have lower performance on the FERET database. The cause of this may be that our method is more robust to changes in the general conditions regarding the image capture procedure. This can be observed by comparing the sets with similar rotations in the FERET and CMU-PIE databases.

Conflict of interest

None declared.

Acknowledgements

This work was supported by FONDECYT 1120613, and by the Department of Electrical Engineering, Universidad de Chile.

References

[1] P. Campadelli, R. Lanzarotti, G. Lipori, Precise eye and mouth localization, Int. J. Pattern Recognit. Artif. Intell. 23 (3) (2009) 359–377.
[2] C. Perez, V. Lazcano, P. Estévez, C. Held, Real-time template based face and iris detection on rotated faces, Int. J. Optomechatronics 3 (1) (2009) 54–67.
[3] C.A. Perez, V.A. Lazcano, P.A. Estévez, Real-time iris detection on coronal-axis-rotated faces, IEEE Trans. Syst. Man Cybern. Part C—Appl. Rev. 37 (5) (2007) 971–978.
[4] C.A. Perez, C.M. Aravena, J.I. Vallejos, P.A. Estévez, C.M. Held, Face and iris localization using templates designed by particle swarm optimization, Pattern Recognit. Lett. 31 (9) (2010) 857–868.
[5] C.A. Perez, C.A. Salinas, P.A. Estévez, P.M. Valenzuela, Genetic design of biologically inspired receptive fields for neural pattern recognition, IEEE Trans. Syst. Man Cybern. Part B—Cybern. 33 (2) (2003) 258–270.
[6] C.A. Perez, G.D. Gonzalez, L.E. Medina, F.J. Galdames, Linear versus nonlinear neural modeling for 2-D pattern recognition, IEEE Trans. Syst. Man Cybern. Part A—Syst. Hum. 35 (6) (2005) 955–964.

[7] M.A. Turk, A.P. Pentland, Face recognition using eigenfaces, in: IEEE Computer Society Conference on Computer Vision and Pattern Recognition (CVPR'91), Maui, HI, USA, 1991.
[8] P.N. Belhumeur, J.P. Hespanha, D.J. Kriegman, Eigenfaces vs. Fisherfaces: recognition using class specific linear projection, IEEE Trans. Pattern Anal. Mach. Intell. 19 (7) (1997) 711–720.
[9] M.S. Bartlett, J.R. Movellan, T.J. Sejnowski, Face recognition by independent component analysis, IEEE Trans. Neural Netw. 13 (6) (2002) 1450–1464.
[10] M. Sharkas, M. A. Elenien, Eigenfaces vs. Fisherfaces vs. ica for face recognition; a comparative study, in: 9th International Conference on Signal Processing (ICSP), Beijing, China, 2008, pp. 914–919.
[11] T. Ahonen, A. Hadid, M. Pietikäinen, Face description with local binary patterns: application to face recognition, IEEE Trans. Pattern Anal. Mach. Intell. 28 (12) (2006) 2037–2041.
[12] S. Biswas, G. Aggarwal, P.J. Flynn, K.W. Bowyer, Pose-robust recognition of low-resolution face images, IEEE Trans. Pattern Anal. Mach. Intell. 35 (12) (2013) 3037–3049.
[13] F. Bianconi, A. Fernández, Evaluation of the effects of Gabor filter parameters on texture classification, Pattern Recognit. 40 (12) (2007) 3325–3335.
[14] D. Gabor, Theory of communication, J. Inst. Electr. Eng. 93 (26) (1946) 429–457.
[15] V. Kyrki, J. Kamarainen, H. Kälviäinen, Simple Gabor feature space for invariant object recognition, Pattern Recognit. Lett. 25 (3) (2004) 311–318.
[16] M. Lades, J.C. Vorbrüggen, J. Buhmann, J. Lange, C. von der Malsburg, R. P. Würtz, W. Konen, Distortion invariant object recognition in the dynamic link architecture, IEEE Trans. Comput. 42 (3) (1993) 300–311.
[17] L. Wiskott, J. Fellous, N. Krüger, C. von der Malsburg, Face recognition by elastic bunch graph matching, IEEE Trans. Pattern Anal. Mach. Intell. 19 (7) (1997) 775–779.
[18] C. Liu, H. Wechsler, Gabor feature based classification using the enhanced Fisher linear discriminant model for face recognition, IEEE Trans. Image Process. 11 (4) (2002) 467–476.
[19] W. Zhang, S. Shan, W. Gao, X. Chen, H. Zhang, Local Gabor binary pattern histogram sequence (LGBPHS): a novel non-statistical model for face representation and recognition, in: Tenth IEEE International Conference on Computer Vision (ICCV'05), Beijing, China, 2005, pp. 786–791.
[20] B. Zhang, S. Shan, X. Chen, W. Gao, Histogram of Gabor phase patterns (HGPP): a novel object representation approach for face recognition, IEEE Trans. Image Process. 16 (1) (2007) 57–68.
[21] Z. Lei, S.Z. Li, R. Chu, X. Zhu, Face recognition with local Gabor textons, in: 2th International Conference on Advances in Biometrics (IBC'07), Lecture Notes in Computer Science, vol. 4642, Seoul, Korea, 2007, pp. 49-57.
[22] S. Xie, S. Shan, X. Chen, X. Meng, W. Gao, Learned local Gabor patterns for face representation and recognition, Signal Process. 89 (12) (2009) 2333–2344.
[23] H. V. Nguyen, L. Bai, L. Shen, Local Gabor binary pattern whitened PCA: a novel approach for face recognition from single image per person, in: Third International Conference on Advances in Biometrics (IBC'09), Lecture Notes in Computer Science, vol. 5558, Alghero, Italy, 2009, pp. 269–278.
[24] J. Zou, Q. Ji, G. Nagy, A comparative study of local matching approach for face recognition, IEEE Trans. Image Process. 16 (10) (2007) 2617–2628.
[25] C.A. Perez, L.A. Cament, L.E. Castillo, Local matching Gabor entropy weighted face recognition, in: Ninth IEEE International Conference on Automatic Face and Gesture Recognition (FG 2011), Santa Barbara, CA, USA, 2011, pp. 179–184.
[26] C.A. Perez, L.A. Cament, L.E. Castillo, Methodological improvement on local Gabor face recognition based on feature selection and enhanced Borda count, Pattern Recognit. 44 (4) (2011) 951–963.
[27] L.A. Cament, L.E. Castillo, J.P. Perez, F.J. Galdames, C.A. Perez, Fusion of local normalization and Gabor entropy weighted features for face identification, Pattern Recognit. 47 (2) (2014) 568–577.
[28] Y. Su, S. Shan, X. Chen, W. Gao, Hierarchical ensemble of global and local classifiers for face recognition, IEEE Trans. Image Process. 18 (8) (2009) 1885–1896.
[29] S. Xie, S. Shan, X. Chen, J. Chen, Fusing local patterns of Gabor magnitude and phase for face recognition, IEEE Trans. Image Process. 19 (5) (2010) 1349–1361.
[30] K.-H. Pong, K.-M. Lam, Multi-resolution feature fusion for face recognition, Pattern Recognit. 47 (2) (2014) 556–567.
[31] V. Blanz, T. Vetter, Face recognition based on fitting a 3D morphable model, IEEE Trans. Pattern Anal. Mach. Intell. 25 (9) (2003) 1063–1074.
[32] S. Romdhani, Face image analysis using a multiple features fitting strategy (Ph. D. thesis), University of Basel, Faculty of Science, Basel, Switzerland, 2005.
[33] P. Paysan, R. Knothe, B. Amberg, S. Romdhani, T. Vetter, A 3D face model for pose and illumination invariant face recognition, in: 6th IEEE International Conference on Advanced Video and Signal Based Surveillance (AVSS 2009), Genova, Italy, 2009, pp. 296–301.
[34] A. Asthana, T.K. Marks, M.J. Jones, K.H. Tieu, M.V. Rohith, Fully automatic pose-invariant face recognition via 3D pose normalization, in: The 2011 IEEE International Conference on Computer Vision (ICCV 2011), Barcelona, Spain, 2011, pp. 937–944.
[35] L. Ding, X. Ding, C. Fang, Continuous pose normalization for pose-robust face recognition, IEEE Signal Process. Lett. 19 (11) (2012) 721–724.
[36] S. Du, R. Ward, Component-wise pose normalization for pose-invariant face recognition, in: IEEE International Conference on Acoustics, Speech and Signal Processing (ICASSP'09), Taipei, Taiwan, 2009, pp. 873–876.
[37] D. González-Jiménez, J.L. Alba-Castro, Toward pose-invariant 2-D face recognition through point distribution models and facial symmetry, IEEE Trans. Inf. Forensics Secur. 2 (3) (2007) 413–429.
[38] J. Heo, M. Savvides, Face recognition across pose using view based active appearance models (VBAAMs) on CMU multi-PIE dataset, in: 6th International Conference on Computer Vision Systems (ICVS'08), Lecture Notes in Computer Science, vol. 5008, Santorini, Greece, 2008, pp. 527–535.
[39] H. Gao, H.K. Ekenel, R. Stiefelhagen, Pose normalization for local appearance-based face recognition, in: Third International Conference on Advances in Biometrics (ICB'09), Lecture Notes in Computer Science, vol. 5558, Alghero, Italy, 2009, pp. 32–41.
[40] A.B. Ashraf, S. Lucey, T. Chen, Learning patch correspondences for improved viewpoint invariant face recognition, in: IEEE International Conference on Computer Vision and Pattern Recognition (CVPR), Anchorage, Alaska, USA, 2008, pp. 1–8.
[41] N. Vu, A. Caplier, Efficient statistical face recognition across pose using local binary patterns and Gabor wavelets, in: IEEE 3rd International Conference on Biometrics: Theory, Applications, and Systems (BTAS'09), Washington, DC, USA, 2009, pp. 1–5.
[42] A. Li, S. Shan, W. Gao, Coupled bias-variance tradeoff for cross-pose face recognition, IEEE Trans. Image Process. 21 (1) (2012) 305–315.
[43] A. Sharma, M.A. Haj, J. Choi, L.S. Davis, D.W. Jacobs, Robust pose invariant face recognition using coupled latent space discriminant analysis, Comput. Vis. Image Underst. 116 (11) (2012) 1095–1110.
[44] H. Zhang, Y. Zhang, T.S. Huang, Pose-robust face recognition via sparse representation, Pattern Recognit. 46 (5) (2013) 1511–1521.
[45] H.-D. Liu, M. Yang, Y. Gao, Y. Yin, L. Chen, Bilinear discriminative dictionary learning for face recognition, Pattern Recognit. 47 (5) (2014) 1835–1845.
[46] T.K. Ho, J.J. Hull, S.N. Srihari, Decision combination in multiple classifier systems, IEEE Trans. Pattern Anal. Mach. Intell. 16 (1) (1994) 66–75.
[47] C.A. Perez, L.E. Castillo, L.A. Cament, Illumination compensation method for local matching Gabor face classifier, in: International Symposium on Optomechatronic Technologies (ISOT), Toronto, ON, Canada, 2010, pp. 1–5.
[48] T.F. Cootes, C.J. Taylor, Active shape models—'smart snakes', in: British Machine Vision Conference (BMVC'92), Leeds, UK, 1992, pp. 266–275.
[49] M.S. Sarfraz, O. Hellwich, Probabilistic learning for fully automatic face recognition across pose, Image Vis. Comput. 28 (5) (2010) 744–753.
[50] A. Asthana, M. Jones, T. Marks, K. Tieu, R. Goecke, Pose normalization via learned 2D warping for fully automatic face recognition, in: British Machine Vision Conference (BMVC), University of Dundee, Dundee, Scotland, UK, 2011, pp. 127.1–127.11.
[51] C.D. Castillo, D.W. Jacob, Wide-baseline stereo for face recognition with large pose variation, in: IEEE Conference on Computer Vision and Pattern Recognition (CVPR), Colorado Springs, CO, USA, 2011, pp. 537–544.
[52] C.R. Goodall, Procrustes methods in the statistical analysis of shape, J. R. Stat. Soc. Ser. B Methodol. 53 (2) (1991) 285–339.
[53] D. Cristinacce, T. Cootes, Feature detection and tracking with constrained local models, in: 17th British Machine Vision Conference (BMVC06), Universities of Edinburgh and Heriot-Watt, Edinburgh, Scotland, UK, 2006, pp. 929–938.
[54] J.M. Saragih, S. Lucey, J.F. Cohn, Deformable model fitting by regularized landmark mean-shift, Int. J. Comput. Vis. 91 (2) (2011) 200–215.
[55] K. Fukunaga, L.D. Hostetler, The estimation of the gradient of a density function, with applications in pattern recognition, IEEE Trans. Inf. Theory 21 (1) (1975) 32–40.
[56] F.L. Bookstein, Principal warps: thin-plate splines and the decomposition of deformations, IEEE Trans. Pattern Anal. Mach. Intell. 11 (6) (1989) 567–585.
[57] X. Xie, K.-M. Lam, An efficient illumination normalization method for face recognition, Pattern Recognit. Lett. 27 (6) (2006) 609–617.
[58] T. Sim, S. Baker, M. Bsat, The CMU pose, illumination, and expression database, IEEE Trans. Pattern Anal. Mach. Intell. 25 (12) (2003) 1615–1618.
[59] R. Gross, I. Matthews, S. Baker, Appearance-based face recognition and light-fields, IEEE Trans. Pattern Anal. Mach. Intell. 26 (4) (2004) 449–465.
[60] X. Chai, S. Shan, X. Chen, W. Gao, Locally linear regression for pose-invariant face recognition, IEEE Trans. Image Process. 16 (7) (2007) 1716–1725.
[61] T. Kanade, A. Yamada, Multi-subregion based probabilistic approach towards pose-invariant face recognition, in: IEEE International Symposium on Computational Intelligence in Robotics Automation, vol. 2, Kobe, Japan, 2003, pp. 954–959.
[62] S.J.D. Prince, J.H. Elder, J. Warrell, F.M. Felisberti, Tied factor analysis for face recognition across large pose differences, IEEE Trans. Pattern Anal. Mach. Intell. 30 (6) (2008) 970–984.

Leonardo A. Cament received the B.S. and P.E. in Electrical Engineering from Universidad de Chile in March 2008 with the highest honors. He is a Ph.D. candidate at the Department of Electrical Engineering, Universidad de Chile. His main interests in research are pattern recognition applied to eye detection, face recognition and human machine interfaces.

Francisco J. Galdames received the B.S. and P.E. in Electrical Engineering and the M.S degree in Biomedical Engineering all from Universidad de Chile in 2006. In 2012 he obtained the Ph.D from Universidad de Chile and Université Joseph Fourier. He is a postdoctoral fellow at Universidad de Chile. His interests include pattern recognition applied to face recognition and 3D modeling.

Kevin W. Bowyer is the Chair of the Department of Computer Science and Engineering at the University of Notre Dame. Professor Bowyer received a 2014 Technical Achievement Award from the IEEE Computer Society, and is a Fellow of the IEEE and the IAPR. His main research interests are in computer vision and pattern recognition, including biometrics, data mining, object recognition and medical image analysis.

Claudio A. Perez received the B.S. and P.E. in Electrical Engineering and the M.S. degree in Biomedical Engineering all from Universidad de Chile in 1980 and 1985, respectively. He was a Fulbright student at the Ohio State University where he obtained the Ph.D. in 1991. He was a visiting scholar at UC, Berkeley in 2002 through the Alumni Initiatives Award Program from Fulbright Foundation. Currently he is a Professor at the Department of Electrical Engineering, Universidad de Chile.